5
Theoretical Analysis of Nanotube Functionalization and Polymer Grafting

Kausala Mylvaganam and Liang Chi Zhang

5.1
Introduction

Carbon nanotubes (CNTs) are considered to be promising materials for many applications in the development of nanotechnology. Some applications, however, are hindered by the difficulties in the dispersion, manipulation, and processability of CNTs, which are highly entangled and form bundles due to van der Waals attraction among the tubes. Hence for technical applications, it is necessary to first disperse them without reducing their aspect ratio such that they can be mixed with other substances effectively to form composites, incorporated into fibers or deposited as a film. A variety of mechanical/chemical/physical methods such as ultrasonication, high shear mixing, chemical modification through functionalization, adsorption of charged surfactants and electrolytes, wrapping with polymers, and complex formation by π–π interactions, have been used to disperse CNTs [1–7]. Functionalization of nanotubes has become attractive for synthetic chemists and material scientists as it not only improves the solubility and dispersion of CNTs but also can expand their potential application areas through the change of mechanical and electrical properties.

Meur *et al.* showed that functionalized polymers offer the possibility to disperse CNTs in organic solvents [8]. Polymers have been attached to single-walled carbon nanotubes (SWCNTs) via "grafting from" and "grafting to" techniques [9, 10]. The "grafting from" method involves first the attachment of polymerization initiators to the surface of SWCNTs (i.e., first functionalizing the nanotubes) followed by polymerization of monomers from the resulting nanotube-based macroinitiator. The advantage of this "grafting from" method is that the polymer growth is not limited by steric hindrance, allowing high-molecular-weight polymers to be efficiently grafted. The "grafting to" method involves the attachment of premade polymer chains to the surface of CNTs. In this strategy, architecturally controlled polymers (linear, block, etc.) that have an active end-group can be used as a linker to the nanotube.

Theoretical studies can be very helpful toward a comprehensive understanding of the nature of the functionalization of CNTs. Computational studies based on

Surface Modification of Nanotube Fillers, First Edition. Edited by Vikas Mittal.

ab-initio quantum mechanics method using density functional theory (DFT), molecular dynamics simulation, and hybrid quantum mechanics/molecular mechanics (QM/MM) have been carried out to investigate the mechanism behind the functionalization of SWCNTs by molecules or molecular groups.

This chapter will discuss various theoretical considerations in functionalizing CNTs and grafting polymers onto CNTs.

5.2 Theoretical Techniques in Modeling Nanotube Functionalization

5.2.1 *Ab-initio* Quantum Mechanics Method

Ab-initio methods are based entirely on first principles. Among the theoretical methods, *ab-initio* calculations are complementary to the information obtained by experiments and in some cases can predict hitherto unobserved phenomena. Hence the *ab-initio* methods have been widely used in the design of new materials. In principle, *ab-initio* methods converge to the exact solutions of the underlying equations as the number of approximations is reduced. However, in practice it is impossible to eliminate all the approximations. To treat large molecules, approximate method such as DFT is used.

A variety of functionals have been developed to account for exchange and correlation terms in DFT [11, 12]. The most widely used functional is the local-density approximation [13] (LDA), where the functional depends only on the density at the coordinate where the functional is evaluated. This functional has been shown to be especially appropriate for studying the adsorption of organic molecules on CNTs. However, it is well known that this functional tends to overestimate binding energies and charge transfer [14]. Hybrid functionals such as B3LYP [15–18] that include a component of the exact exchange energy are known to produce reasonable results for bond lengths, bond angles, and bond energies for a wide range of molecules [19]. Sections 5.3–5.5 will describe a few examples where these functionals are used in the study of CNT functionalization and subsequent polymer grafting. Even though the DFT method uses functionals that involve parameters derived from empirical data, they are considered to be *ab-initio* for determining molecular electronic structures of materials. The DFT methods including different functionals have been incorporated in popular commercial quantum mechanical software such as Gaussian 09, DMol3, VASP, SIESTA code, etc.

5.2.2 Molecular Dynamics Modeling

Molecular dynamics simulation has been widely used in understanding and characterizing the properties of CNTs. However, such simulations have to be done carefully to achieve the best representation of reality. It is important to select an appropriate interaction potential that effectively describes the deformation of a

nanotube correctly. During a loading process, an improper treatment of the temperature rise can lead to fictitious results. In molecular dynamics, heat conduction is accomplished via the so-called thermostat atoms and various thermostatting methods. For small systems that are practical for molecular dynamics studies, the adiabatic relaxation method often leads to a fluctuation of the vibrational–relaxation rate. In isokinetic thermostatting, the temperature is maintained in different ways. For example, in the Berendsen thermostat scheme with velocity scaling, the velocities of thermostat atoms are scaled to fix the total kinetic energy. In the Gaussian feedback or Evans–Hoover (EH) scheme with force scaling, however, the kinetic energy is monitored and information is fed back into the equations of motion so that the kinetic energy is kept constant to dissipate heat by controlling the thermostatting force. The velocity scaling has been used in general because it is a simpler scheme to implement. For small time steps, the Gaussian isokinetic method and velocity scaling method are identical. However, a very small time step will give an unusually high loading rate. On the other hand, a small displacement step with a small time step will be computationally expensive. The flaw in the isokinetic–thermostatting method is that it is impossible to separate the effects of thermostatting on rate processes. In addition, a system has to be relaxed initially as well as during the simulation so that the velocities of the Newtonian and thermostat atoms reach equilibrium at the specified temperature of simulation; thus appropriate time step and displacement step have to be selected to get a reasonable loading rate.

Hence in the rest of this section, the necessary details such as the potential, number of thermostat atoms, thermostat method, time step, displacement step, and the number of relaxation steps that are central to a reliable simulation of nanotube will be discussed.

In order to examine the reliability of simulations, we will compare and discuss the stress–strain relationship of single-walled zigzag (17,0) and armchair (10,10) nanotubes obtained with different schemes. The simulations were carried out at 300 K with Berendsen (B) and EH thermostats and a time step of 0.5 fs with the interatomic forces described by Tersoff [20, 21] and Brenner [22, 23] potentials under Schemes I and II as described below.

5.2.2.1 Scheme I

In this scheme, the first two layers of atoms on both ends of a CNT were held rigid. The next four layers were taken as thermostat atoms and the remaining were treated as Newtonian atoms. First, the tubes were annealed at the simulation temperature for 5000 time steps. Then the rigid atoms on both ends were pulled along the axial direction with incremental steps of 0.05 Å. Each displacement step was followed by 1000 relaxation steps in order to dissipate the effect of preceding displacement step over the entire length of the tube.

5.2.2.2 Scheme II

In this scheme, all atoms except the rigidly held boundary ones were treated as thermostat atoms. In this case, each displacement step was followed by 50 relaxation steps.

The simulation parameters had a remarkable influence on the results. Different schemes led to significantly different stress–strain curves (Figure 5.1) and necking processes (Figure 5.2). The simulation using Tersoff–Brenner potential and Berendsen thermostat with all atoms as thermostat atoms with 50 relaxations steps after each displacement of 0.008 Å is a reliable and cost-effective method [24].

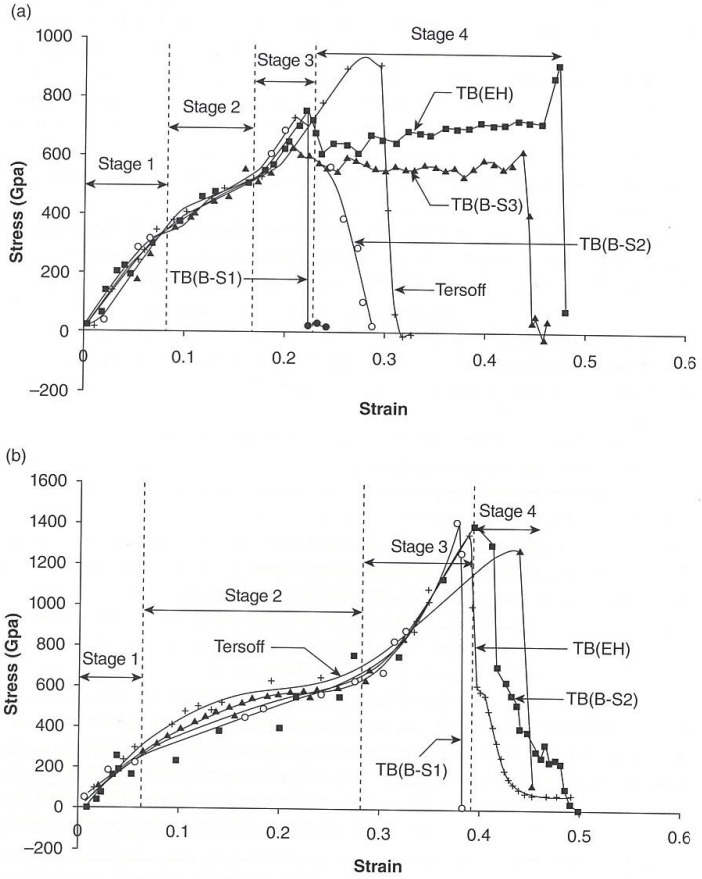

Figure 5.1 The stress–strain curves of (a) a (17,0) zigzag SWCNT and (b) a (10,10) armchair SWCNT using Tersoff and Tersoff–Brenner potentials. In the figure, TB(B-S1) is the calculation with Berendsen thermostat and Scheme 1 simulation details; TB(B-S2) is the calculation with Berendsen thermostat and Scheme 2 simulation details and TB(B-S3) is the calculation as in TB(B-S2) but with a smaller displacement step of 0.008 Å. TB(EH) is the calculation with Evans–Hoover thermostat. Reprinted from [24] with permission.

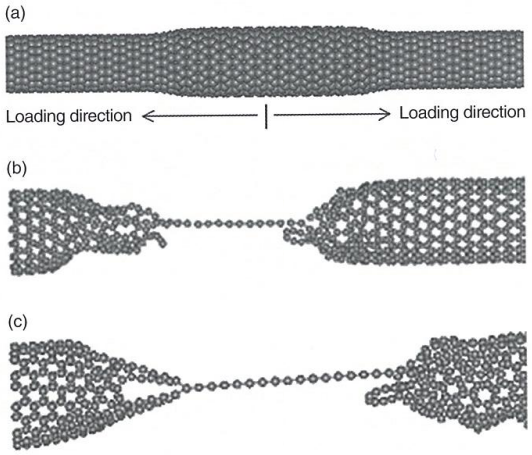

Figure 5.2 (a) Deformation of a zigzag SWCNT, TB(B-S3) calculation showing the propagation of necking. (b) Atomic chain of a zigzag tube when using Berendsen thermostat. (c) Atomic chain of an armchair tube when using Berendsen thermostat. Reprinted from [24] with permission.

5.2.3
Hybrid QM/MM Approach

Ab-initio quantum mechanics (including DFT) procedures are expensive for routine calculations even for a simple system like a CNT. While semiempirical methods, such as molecular dynamics, molecular mechanics, are useful and accessible tools to describe the properties of CNTs semiquantitatively, they are unable to provide reliable estimate for the energetics of reaction mechanisms. A hybrid QM/MM approach solves this problem to a certain extent. It has been implemented in popular commercial software such as Gaussian 09, DMol3, etc. In this approach, a whole molecular system is divided into two or three levels. A relatively small section (usually the reaction center) is treated at a more accurate *ab-initio* level and the rest is treated with a computationally less demanding (molecular mechanics or other semiempirical) method. A couple of examples discussed in Section 5.4 use this approach.

5.3
Functionalizing Carbon Nanotubes through Mechanical Deformation

Tension, compression, torsion, and pure bending are fundamental modes to deform CNTs under certain external conditions of mechanical loading. Theoretical

studies have shown that the ridges of a deformed CNT bind functional groups tightly with high binding energy but binding with the deformation-flattened surface is weak–even weaker than that of a nondeformed nanotube. Mylvaganam and Zhang [25] simulated the deformation of (17,0) zigzag nanotubes by molecular dynamics simulation and then revealed the reactivity of the deformed nanotube sections with radicals via optimizing its geometry while keeping the geometry of the deformed tube section fixed, using *ab-initio* DFT with a hybrid functional B3LYP [15–18] and a 3-21G basis set [26]. Before optimizing the geometry, hydrogen atoms had been added to the dangling bonds of the perimeter carbons. The following sections will compare and discuss the reactivity of hydrogen and alkyl radicals with CNT deformed under the above-mentioned fundamental deformation modes.

5.3.1 Tension

Under this type of loading, the nanotube stretched along the loading direction and then necked. The necking propagated over the entire length of the tube and formed one atom chain before breaking into two pieces. Tensile loading does not generate ridges and flat surfaces like other loadings. Hydrogen atom binding with sections of tubes having low strain energy of 2.22 kJ/mol and high strain energies of 15.71 and 37.21 kJ/mol were investigated by quantum mechanics study. The hydrogen atom binding energy with the low strain energy section is 245.9 kJ/mol and with the high strain energy section is 258.5 kJ/mol (Figure 5.3).

5.3.2 Compression

Under compression loading, the tube started buckling once it reaches the strain energy of 21.82 kJ/mol. After this, the strain energy started to decrease and increase

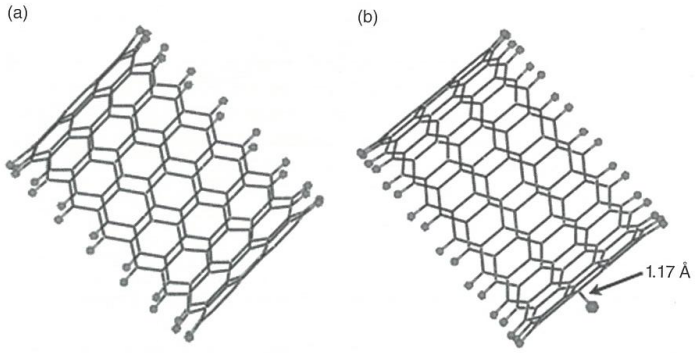

Figure 5.3 (a) Section of the CNT under tensile deformation and (b) optimized structure of the hydrogen radical on the deformed section of the CNT. Reprinted from [25] with permission.

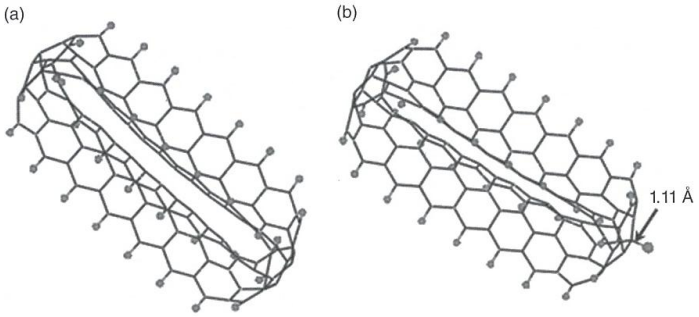

Figure 5.4 (a) Section of the CNT under compressive deformation (strain = 0.135) with the hydrogens at the dangling bonds of the perimeter C atoms optimized at DFT/3-21G level and (b) optimized structure of the hydrogen radical at the ridge. Reprinted from [25] with permission.

as it forms more buckles. Sections of the tube having strain energies of 2.01 kJ/mol (before buckling) and 23.06 kJ/mol (soon after buckling) were used in quantum mechanics study. The section of the compressed tube, with the hydrogen atoms added to the dangling bonds of the perimeter C atoms, is shown in Figure 5.4a. The hydrogen atom placed near the ridge of these sections binds to one of the C atoms with binding energies of 269.5 (before buckling) and 480.4 kJ/mol (after buckling; Figure 5.4b). Before buckling, when the strain energy was 2.01 kJ/mol, the curvature of the tube did not change significantly and hence the binding energy was low.

5.3.3 Torsion

Under this type of deformation mode, the strain energy varied initially cubically with the twisting angle. At the onset of buckling, the energy dropped a little and then changed almost linearly. The buckling started at the strain energy of 7.28 kJ/mol, before which the tube retained its cylindrical shape. Sections of the deformed CNT under the strain energy of 1.97 (before buckling) and 8.51 kJ/mol (soon after buckling) were used in the quantum mechanics study. Figure 5.5a shows a section of the tube after buckling, having clear ridges formed on twisting, with H atoms added and optimized to the dangling bonds of the perimeter C atoms. On placing a hydrogen atom near to those tube sections and optimizing its geometry, the hydrogen atom tightly bound to one of the carbon atoms at a ridge with binding energies 229.9 (before buckling) and 427.1 kJ/mol (after buckling), respectively. The optimized geometry of the hydrogen bound nanotube section after buckling is shown in Figure 5.5b. The shorter bond lengths and higher binding energies compared to the hydrogen radical attached to the nondeformed tube shows that the deformation promotes the reactivity. This could be explained

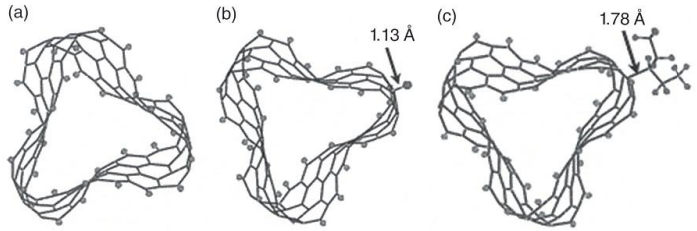

Figure 5.5 (a) Section of the CNT under 40° torsional deformation with the hydrogens at the dangling bonds of the perimeter C atoms optimized at DFT/3-21G level, (b) optimized structure of the hydrogen radical at the ridge, and (c) optimized structure of the C_5H_{11} radical at the ridge. Reprinted from [25] with permission.

by the change in hybridization of C atoms. On twisting the nanotube, some of the sp^2 hybridized carbon atoms become sp^3 and hence one of the sp^3 hybridized orbitals is free to form a covalent bond with an incoming atom or molecule. On a nondeformed tube, the C atoms have only a slight sp^3 character due to its cylindrical shape of the tube, which gives rise to a weak bond with a low binding energy.

On placing an alkyl radical (C_2H_5–$\dot{C}H$–C_2H_5) near to one of the C atoms at the ridges of the nanotube section of Figure 5.5a, and optimizing its geometry, the radical bound to the C atom, as shown in Figure 5.5c with a binding energy of 337.6 kJ/mol. On the other hand, the binding energy between the alkyl radical and a deformation-free nanotube is only 4.3 kJ/mol with CNT-alkyl C–C bond length of 3.7 Å, that is, the alkyl radical does not bind to free nanotube.

5.3.4
Bending

Under pure bending, the tube started kinking after reaching a strain energy of 1.88 kJ/mol. Sections of the tube under a strain energy of 1.88 (just before kinking) and 2.95 kJ/mol (soon after kinking) were used in the quantum mechanics study. The center section (kink site) with the hydrogen atoms added to the dangling bonds of the perimeter C atoms is shown in Figure 5.6a. Here again it has the ridges and flattened portion. The hydrogen atom placed near to the ridge bound to one of the C atoms at the ridge with binding energies of 232.0 (before kinking) and 398.9 kJ/mol (after kinking; Figure 5.6b). Although due to ovalization the curvature of the tube changes before kinking, it did not form well-developed ridge and flat surface. Thus the binding energy of radicals was low before kinking.

In summary, quantum mechanics calculations showed that the radicals strongly bind to the C atoms at the ridges; flattened surfaces show even a lower binding

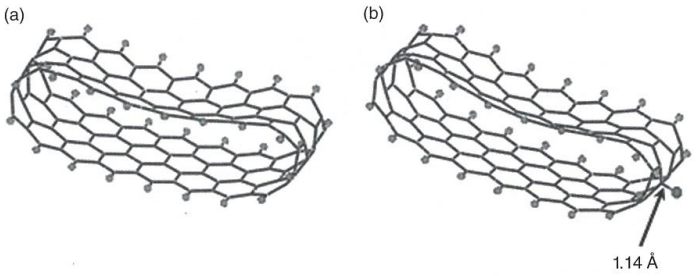

Figure 5.6 (a) Section of the NT under 40° bending deformation with the hydrogens at the dangling bonds of the perimeter C atoms optimized at DFT/3-21G level and (b) optimized structure of the hydrogen radical at the ridge. Reprinted from [25] with permission.

strength compared to the free tube as their behavior approaches that of a graphite sheet. Under torsion, the ridges are formed along the entire length of the tube and this gives a higher binding energy under relatively low strain energy. Thus this appears to be the best deformation mode to promote multiple reactions on nanotubes. Srivastava *et al.* [27] also predicted that the chemisorption of hydrogen atoms is enhanced by ~1.6 eV (i.e., ~154.4 kJ/mol) at regions of high deformation due to bending and torsion of SWNTs. In the blending of CNT–polymer composites, a CNT is often under a combined loading including many of the loading modes studies above. Furthermore, because of the large aspect ratio of CNTs, multiple kinking/buckling (can be hundreds) may form on a single CNT. These, according to the above discussion, will enhance the formation of chemical bonds. Thus mechanical deformations in composite blending can promote reactivity with nearby chemical species.

5.4
Functionalizing Carbon Nanotubes via Chemical Modification

Chemical functionalization offers an efficient route not only to modify the chemical and physical properties of CNTs but also to further expand their potential application areas. The main approaches for functionalizing CNTs through chemical modification can be grouped into two main categories – covalent attachment of chemical groups and noncovalent adsorption or wrapping of functional molecules onto the tubes.

5.4.1
Covalent Modification

Covalent functionalization of CNTs allows functional groups to be attached to tube ends or sidewalls. When chemical groups are attached to CNTs through

covalent bonds, the nanotube carbon atoms are chemically modified. Excessive modification of the CNTs can ruin the tubular framework and thereby reduce its mechanical strength. On functionalizing CNTs by acid treatment, carboxylic acid groups are introduced on the surface of CNTs that leads to stabilization in polar solvents and helps to covalently link amides, amines, polymers, and other groups. However, the acids attack defective sites of the CNTs and cut them into many short nanotubes, thereby decreasing their aspect ratios. Despite this, covalent modification of CNTs has been spotted as a viable route to broaden possible applications. Some details are discussed below.

5.4.1.1 Functionalization with Fluorine

Fluorination of CNTs was one of the first sidewall functionalization reactions in 1996 [28]. Jaffe [29] used *ab-initio* quantum chemistry approach for the chemical modification of CNT sidewalls with fluorine. Owing to the large size of complete segments on CNTs, Jaffe used polycyclic aromatic hydrocarbon molecules with curvature maintained by external constraints to represent pieces of (10,10), (5,5), and (16,0) nanotubes. DFT calculations with a B3LYP functional and a 6-31G(d) basis set showed that the F atoms preferred to bond next to each other. The use of small hydrocarbons to simulate a nanotube sidewall can yield insight into the bonding, but the best model might not always be obvious. For example a complete geometry optimization at the reaction site is important but it would result in the hydrocarbon becoming planar and hence it would not reflect the nanotube sidewall. Bauschlicher [30, 31] used the hybrid QM/MM approach to study the hydrogen and fluorine binding to the sidewall of a (10,0) CNT, where a two-level ONIOM approach (developed by Morokuma and coworkers [32]) in which molecular mechanics is used to treat a sizable segment of the nanotube and DFT(B3LYP) is used to study the area where F or H atom attaches to the sidewall, thus eliminating the constraints used in Jaffe's work. These calculations also showed the F atoms appear to favor bonding next to existing F atoms. Similar to fluorinated fullerenes [33], SWCNTs once fluorinated can serve as a staging point for a wide variety of sidewall chemical functionalizations. By treating fluorinated tubes with strong nucleophiles such as Grignard reagents, alkyl lithium reagents, and metal alkoxides, the fluorine substituents were replaced and derivatized products, for example, methyl-, butyl-, hexyl-, and methoxylnanotubes, were formed [34, 35].

5.4.1.2 Functionalization with Carboxylic Group, Amine Group, and Amide Group

Veloso *et al.* [36] functionalized SWCNTs by investigating the interaction of –COOH, $–NH_2$, and $–CONH_2$ groups with an (8,0) SWCNT using total energy *ab-initio* calculations based on DFT adopting a generalized gradient approximation for the exchange and correlation terms. All three functional groups induced local distortions along the radial directions on the tube sidewall due to the local sp^3 hybridization of the C–C or C–N bonding between the C atom of the tube and the C or N atoms of the functional group, demonstrating covalent bonds between the SWCNT and the functional groups as shown in Figure 5.7a–c. These covalently

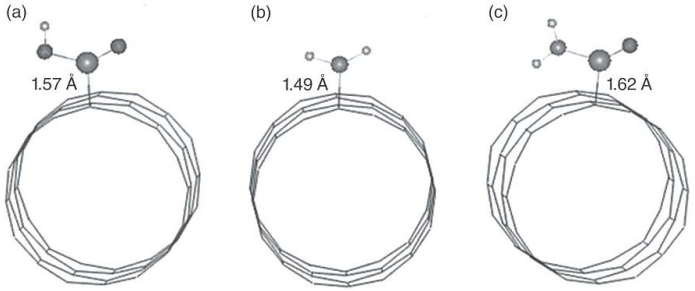

Figure 5.7 Structural configurations of the sidewall functionalization: (a) SWCNT–COOH, (b) SWCNT–NH_2, (c) SWCNT–$CONH_2$.

functionalized CNTs are promising materials for catalysis, electronic and optic devices, sensors, gas storage, and making high-performance composites.

5.4.1.3 Functionalization with Nitro Group

Mercuri and Sgamellotti [37] exploited the sidewall functionalization of CNTs with NO_2, as a way to develop gas-sensing devices. The adsorption of NO_2 on the sidewall of CNT was modeled by performing a hybrid QM/MM calculation. They analyzed the interaction of NO_2 (i) with the perfect hexagonal framework of CNT sidewall, (ii) with CNT having Stone–Wales defect constituting two adjacent pentagon–heptagon ring pairs, originating from the rotation of a single C–C bond on the hexagonal network of the sidewall by 180°, and (iii) with a site originating from the vacancy of carbon atom on the sidewall considering the "nitro" attack and "oxo" attack individually. The results indicated a low tendency to adsorption of NO_2 for the perfect hexagonal network of the sidewall. Chemisorption on the Stone–Wales defects is slightly favored compared to the defect-free sidewall showing that the defects can partially account for the gas-sensing action. In the "nitro" configuration, the interaction between NO_2 to the sidewall at the vacancy indicated a strong chemisorption; for the "oxo" attack, the results suggested the dissociation of NO_2 at the vacancy with the formation of a new C–O bond and the release of an NO molecule. Experimental results also indicated a larger tendency to reaction for more defected CNTs and the presence of C–N and carbonyl groups, upon exposure to NO_2.

5.4.1.4 Functionalization with Transition Metal Complex

New directions for the functionalizations have been opened by the extension of transition metal chemistry to the interaction with the CNT sidewall. Mercuri and Sgamellotti [38] investigated the interaction of SWCNTs with Vaska's complex [39] (*trans*-$Ir(CO)Br(PPh_3)_2$–an electron-rich transition metal complex) by means of hybrid QM/MM calculations in which Vaska's complex and a portion of CNT

sidewall (~16–24 carbon atoms) were included in the QM part. For the MM part, the Tripos force field [40] that is known to give good results for π–π interactions and for the QM part, DFT with Becke [15] and Perdew [41] corrections that gives a good description of the metal–ligand interaction were used. Investigation of the interaction between the complex and (i) the defect-free sidewall, (ii) capped-end, and (iii) pentagon–heptagon defect showed that the defect-free sidewall is almost inert to coordination with the transition metal. However, nanotube end-caps or defective sites show higher tendency to coordination with the inorganic fragment, which indicate that a stable adduct is likely to be formed when at least one of the coordinating carbon atoms belongs to a pentagonal ring. Thus CNTs can be functionalized with transition metal complexes. The formation of a stable adduct has been experimentally evidenced by Banerjee and Wong [42].

5.4.1.5 Functionalization via the Introduction of Free Radical

Mylvaganam and Zhang [43] studied the reaction of a simple oxy radical $^{\bullet}OCH_3$, with a (5,0) zigzag nanotube segment having 60 C atoms (length = 11.36 Å) with hydrogen atoms added to the dangling bonds of the perimeter carbons by fully optimizing the geometry using DFT with a hybrid functional B3LYP and a 3-21G basis set. The optimized geometry of the $C_{60}H_{10}$–OCH_3 radical (Figure 5.8) show the newly formed C–O covalent bond having a bond length of 1.463 Å. The three C–C bonds radiating from the substituted sp^3 carbon of the nanotube are lengthened to ~1.5 Å. The newly formed nanotube-bound radical is delocalized over several nanotube carbon atoms and is stabilized by ~168 kJ/mol. This value is likely to increase with the addition of polarization functions to carbon atoms.

5.4.1.6 Functionalization via the Introduction of Anion

Reaction of secondary butyl anion ($CH_3CH^-CH_2CH_3$) with the nanotube model $C_{60}H_{10}$ was studied by fully optimizing the geometry at the DFT(B3LYP)/3-21G level. The optimized geometry of the $C_{60}H_{10}$–C_4H_9 anion is presented in Figure 5.9. This anion is lower in energy compared to its corresponding reactants by

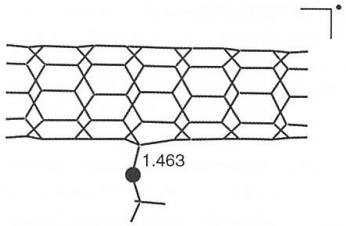

Figure 5.8 DFT(B3LYP)/3-21G optimized geometry of $C_{60}H_{10}$–OCH_3 radical. Note that the solid sphere within the molecular framework represents an oxygen atom. Reprinted from [43] with permission.

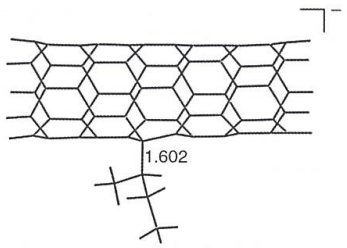

Figure 5.9 DFT(B3LYP)/3-21G optimized geometry of $C_{60}H_{10}$–C_4H_9 anion [43].

~514 kJ/mol. This shows that the CNT can be functionalized with the standard anionic initiator butyl lithium and the resulting CNT anion is very stable.

Nanotubes modified through covalent bonds via the introduction of radicals or anions (methods (e) and (f)) can serve as initiators for the *in-situ* polymerization process that can further lead to polymer-grafted CNT composites.

5.4.2 Noncovalent Modification

A CNT surface can be modified via van der Waals forces and π–π interactions, by adsorption or wrapping of poly-nuclear aromatic compounds, surfactants, polymers, or biomolecules. The main advantage is that chemical functionalities can be introduced to the CNTs without affecting the structure and electronic network of the tubes. Unlike the covalent modifications described above, which introduce defects in the form of sp^3 hybridized carbons that can cause loss of remarkable thermal, electrical, and mechanical properties of CNTs, the noncovalent modification also known as supramolecular functionalization preserves the above properties and enables the utilization of nanotubes in their unmodified state.

5.4.2.1 $CHCl_3$ Adsorption

Girao *et al.* [44] functionalized SWCNTs through chloroform adsorption. As grown, CNTs generally show several defects. Single vacancies are found to be the most important structural defects in CNTs since they significantly promote changes in the physical and chemical properties of the nanotubes. Scientists investigated the reaction of $CHCl_3$ with pristine, and defective SWCNTs in (i) "atom" configuration where the H atom or Cl atom is placed directly above a C atom of the nanotube surface, (ii) "ring" configuration where the H or Cl atom interacts with the SWCNT ring, (iii) "net" configuration where each one of the three Cl atoms is situated on the center of the nanotube ring, (iv) vac-A configuration, where one Cl atom close to the vacancy, and (v) vac-B configuration where three Cl atoms close to the vacancy. Using first principles calculations based on

DFT adopting LDA to account for exchange and correlation terms, they predicted a physisorption regime in all cases. This shows that SWCNTs are promising materials for extracting trihalomethanes from the environment. The stability of the SWCNT–CCl_2 is comparable with SWCNT–COOH system and is in agreement with FTIR and Raman scattering experiments.

5.4.2.2 Adsorption of Metalloporphyrin Complexes

In porphyrins, the flat planar aromatic structures are ideal for π-stacking interactions with the sidewalls of SWCNTs and they play an important role in industry, technology, and biological systems [45]. Compared to porphyrin–SWCNT complexes, the supramolecular metalloporphyrin–SWCNT systems have more interesting magnetic, optic, and spintronic properties, suggesting wider applications such as designing novel biosensors, catalysts, and spintronic molecular devices. Zhao and Ding [46] investigated the interaction of metalloporphyrins (CoP, NiP, CuP, and ZnP) molecules with zigzag (10,0) and armchair (6,6) SWCNTs using DFT within the generalized gradient approximation of the Perdew–Burke–Ernzerhof functional [47], which is proven to give good description for the nature of intermolecular bonding [48]. They found that the adsorption energies of metalloporphyrin functionalized semiconducting (10,0) tubes varied from −0.59 to −0.61 eV and metallic (6,6) tubes varied from −0.43 to −0.51 eV, depending on the identity of the center metal of metalloporphyrin. The closest metal–tube distances were in the range of 3.15–3.3 Å for semiconducting tube and 3.4–3.6 Å for metallic tube. These results showed that the adsorption of metalloporphyrin complexes on semiconducting SWCNTs is much stronger than that on the metallic SWCNTs. In addition, the charge transfer from metalloporphyrin molecules to the (10,0) SWCNT is significantly larger than that to the (6,6) SWCNT. Hence the semiconducting tubes can be separated from metallic tubes through the adsorption of metalloporphyrin. Moreover, irrespective of the tube's chirality, CoP–SWCNT and CuP–SWCNT complexes showed a net magnetic moment because of the presence of the unpaired electrons, making them possess interesting magnetic and optic properties. For the above purposes, it is vital to functionalize the sidewalls of SWCNTs with metalloporphyrin molecules, which is critical to the physical properties of SWCNTs and their applications.

5.4.2.3 Interaction of Aromatic Amino Acids

Noncovalent interactions of biological molecules have potential applications in molecular electronics, as biosensors and chemical sensors. Electrical conductance of CNTs changes appreciably as proteins are immobilized on their sidewalls [49]. Studies on the structure–function–affinity of peptides with CNTs have shown that the aromatic amino acid phenylalanine has an important role in the enhancement of the adsorption properties of CNTs [50]. Rajesh *et al.* [51] investigated the nature of interaction of four aromatic amino acids (phenylalanine, histidine, tyrosine, and tryptophan) with CNTs, which has implications toward developing biosensors, through *ab-initio* calculations. They have used DFT within the generalized gradient approximation as implemented in Vienna *ab-initio* simulation package (VASP) for geometry optimizations and Moller–Plesset second-order perturbation theory (MP2) using a 6-31G* basis set to get more accurate prediction of the interaction between the amino acids and CNTs. These studies showed that the aromatic rings of the amino acids prefer to orient in parallel with respect to the plane of the CNTs, which bears the signature of weak π–π interactions. In addition, the strength of the interaction was found to be in excellent correlation to the polarizability of the aromatic motifs of the amino acids.

5.4.2.4 Encapsulation of Organic Molecules

For molecular electronic applications, it is essential to obtain both p- and n-type air-stable CNTs. SWCNT filed-effect transistors under ambient conditions are p-type due to electron withdrawing by the absorbed oxygen. Thus the production of n-type air-stable CNT transistors is technologically important.

Air-stable amphoteric doping has been realized by encapsulating organic molecules inside SWCNTs. On tuning the electron affinity or ionization potential of the encapsulated molecules, researchers have shown that both p- and n-type doping of CNTs can be realized [52, 53]. Encapsulation of electrophilic organic molecules realizes a controllable p-type doping, whereas nucleophilic organic molecules lead to controllable n-type doping. Lu *et al.* [52] modeled the doping of a zigzag (16,0) SWCNT with electrophilic organic molecules such as tetracyano-*p*-quinodimethane and tetraflurocyano-*p*-quinodimethane and nucleophilic organic molecule such as tetrathiafulvalene using DFT. They find that these molecules are physisorbed inside the nanotube.

Sa *et al.* [53] investigated the functionalization of an armchair (8,8) SWCNT by tetrathiafulvalene and found that the external absorption is less stable than the encapsulation one. The molecule is physisorbed (i.e., no covalent bonding between the molecule and the CNT) inside the tube. Mulliken population analysis showed that tetrathiafulvalene molecules are electron donators to the armchair nanotube. This charge transfer induces an ambipolar system and the resulting electrostatic interaction may play a role for its stability.

5.5 Polymer Grafting

It is known that the radicals and negative charges generated on fullerene C_{60} can serve as initiators for further reactions with alkenes or epoxides that lead to the formation of polymer-grafted fullerene [54, 55]. Based on this, a few papers discussed chemically functionalizing nanotubes via the introduction of radicals or anions that can serve as initiators for the *in-situ* polymerization process, which can further lead to polymer-grafted CNT composites [4, 10, 56, 57]. Each of these functionalization methods has their own merit. In synthesizing different polymers, different initiators are used following different mechanisms. For example, polyethylene (PE) is prepared by free radical addition polymerization as described

Scheme 1

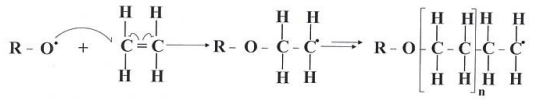

Scheme 2

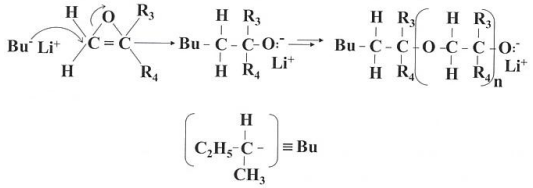

Figure 5.10 Free radical addition (Scheme 1) and anionic (Scheme 2) polymerization schemes.

in Scheme 1 of Figure 5.10, whereas polystyrene and polyepoxide are prepared by anionic polymerization as described in Scheme 2 of Figure 5.10.

5.5.1 Grafting Polyethylene

5.5.1.1 "Grafting from" Technique

Mylvaganam and Zhang [43] studied the reaction of C_2H_4 monomer with CNT–methoxy radical formed via the introduction of $^{\bullet}OCH_3$ (i.e., free-radical-functionalized CNT) by fully optimizing the geometry of the reactants and products using the DFT. This led to the formation of a new radical ($C_{60}H_{10}$–OCH_3–C_2H_4 radical, Figure 5.11a) that is 131 kJ/mol lower in energy than the reactants. According to the Mulliken spin density analysis [59], the free electron is mainly localized on the carbon at the free end of C_2H_4, indicating that the resulting radical is ready to undergo a propagation reaction with another C_2H_4 monomer. Addition of a second C_2H_4 molecule formed a bond with the C atom where the free electron was localized showing the typical propagation step in polymerization. The optimized geometry is shown in Figure 5.11b. The new radical is 107.8 kJ/mol lower in energy compared to the reactants. Thus the radical generated on the nanotube acts as an initiator so that a PE chain could be grafted onto the nanotube via *in-situ* polymerization.

5.5.1.2 "Grafting to" Technique

Fullerene can be free radically grafted onto saturated hydrocarbon polymers such as ethylene–propylene copolymer by heating them to 150 °C in the presence of *tert*-butyl peroxide [55]. CNTs are fullerene-related structures. Moreover, in general peroxides are capable of abstracting hydrogen atoms from polymer chains. On the

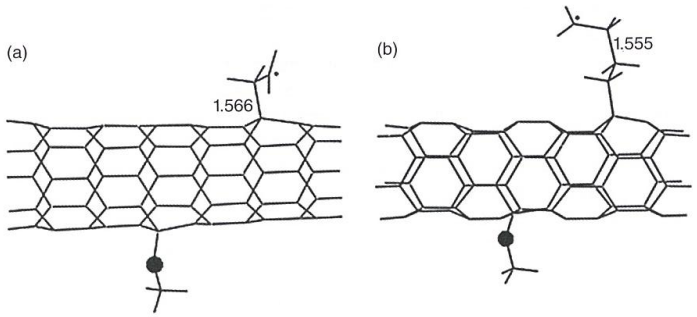

Figure 5.11 DFT/B3LYP optimized structure of (a) $C_{60}H_{10}$–OCH_3–C_2H_4 radical, (b) $C_{60}H_{10}$–OCH_3–CH_2–CH_2–CH_2–CH_2 radical. Reprinted from [58] with permission.

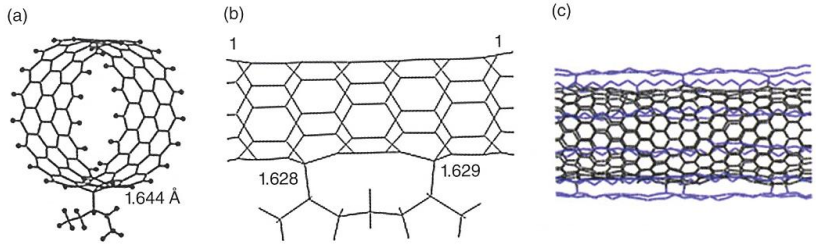

Figure 5.12 (a) DFT/B3LYP(3-21G) optimized structure of SWCNT–C_5H_{11}, (b) DFT/B3LYP(3-21G) optimized structure of SWCNT–C_7H_{14} biradical, (c) a section of molecular dynamics energy minimized structure of SWCNT–PE chains (PE backbone chains are shown in blue) [58, 60].

basis of the above idea, the possible chemical bond formation between the CNT and PE chain radicals was explored using model compounds [58]. Nanotube–polyethylene chain models were generated and investigated by quantum mechanics and molecular dynamics methods. The quantum mechanics calculations used a segment of a CNT with hydrogen atoms added to the dangling bonds of the perimeter carbons and alkyl radicals ($C_5H_{11}^{\bullet}$ and C_7H_{14} biradical with unpaired electrons on the 2nd and 6th carbon atoms) to represent the PE chains. The geometrical parameters were fully optimized using DFT with a hybrid functional B3LYP and a 3-21G basis set. A new C–C bond formed between the section of the nanotube sidewall and the alkyl radical ($C_5H_{11}^{\bullet}$) with a bond length of 1.644 Å demonstrating a covalent bond formation and the bonding at the attachment carbon become tetrahedral with elongated C–C bonds from the attachment site to neighboring carbon atoms (Figure 5.12a). Two new covalent bonds formed with

bond lengths of 1.629 and 1.628 Å between CNT sidewall and C_7H_{14} biradical (Figure 5.12b).

In the molecular dynamics method, 12 PE chains, with each having 56 methylene groups, were placed around a (17,0) CNT of about 75 Å long. Five hydrogen atoms at equal distances along each PE chain were removed to generate radical centers (typically peroxides are capable of doing this). On minimizing the energy by conjugate gradient method, several new C–C bonds between the PE chains and CNTs were formed (Figure 5.12c).

Thus both the calculations at the molecular dynamics and quantum mechanics scales demonstrate that it is possible to form chemical bonds between the PE chains and the CNT by introducing radicals on the PE chains. In principle, radicals can be generated on PE chains by chemical or radiation attack. For example, an oxy radical formed by the pyrolysis of peroxide is capable of abstracting a hydrogen atom on the polymer chain. This method involves the attachment of premade polymer chains to the surface of CNTs (i.e., "grafting to" method).

5.5.2
Grafting Polypropylene Oxide

DFT studies of the reaction of propylene oxide with CNT–secondary butyl anion formed via the introduction of secondary butyl anion (i.e., the anion-functionalized CNT) resulted in the new $C_{60}H_{10}$–C_4H_9–propylene oxide anion as shown in Figure 5.13a. The new C–C bond length is 1.563 Å and the CNT anion attacks the methylene carbon of the propylene oxide. Here the reactants and the products have almost the same energy. The Mulliken charge density analysis showed that a portion of the negative charge is on the oxygen atom, indicating that the resulting anion can react with another propylene oxide monomer so that the reaction can propagate.

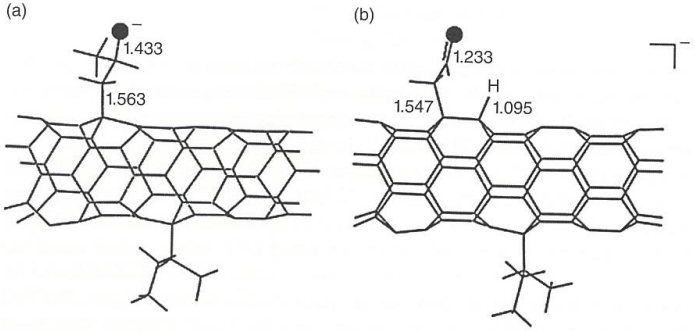

Figure 5.13 DFT/B3LYP optimized geometry of (a) $C_{60}H_{10}$–C_4H_9–propylene oxide anion and (b) $C_{60}H_{10}$–C_4H_9–ethylene oxide anion. Reprinted from [43] with permission.

Thus the anion generated on the CNT act as an initiator so that a poly propylene oxide chain could be grafted onto the nanotube via *in-situ* polymerization.

On the other hand, the reaction of anion-functionalized CNT with ethylene oxide resulted in a $C_{60}H_{10}$–C_4H_9–ethylene oxide anion as shown in Figure 5.13b. Unlike the reaction with propylene oxide, in this case although the epoxide ring opened up as in Scheme 2 of Figure 5.10, but the C–O bond shortened to –C=O and lost one hydrogen to the nanotube. As a result, the oxygen atom no longer possesses a negative charge for the reaction to propagate. This means that grafting a PE oxide chain onto nanotube via anionic polymerization may not be feasible. Thus the *ab-initio* DFT calculations are capable of predicting whether a reaction will take place or not.

5.5.3
Grafting Oligo-N-Vinyl Carbazole

Poly vinyl carbazole has interesting photoconductive properties [61, 62]. As such, very recently, Zaidi *et al.* [63] explored grafting of short-oligo-*N*-vinylcarbazole (OVK) onto SWCNTs by performing different experimental analyses (optical absorption, photoluminescence, infrared, and Raman) and theoretical studies based on *ab-initio* and semiempirical AM1 [64] methods. The structures of OVK having four VK units and a section of SWCNT having a diameter of 1.3 nm had been fully optimized at the DFT(B3LYP)/3-21G* level. The structure and the infrared vibrational frequencies of OVK-SWCNTs composite were calculated at the *ab-initio* Hartree–Fock and semiempirical AM1 level, which is an effective tool for qualitative study of functionalized nanotubes [65]. Zaidi *et al.* compared the force constants between neighboring atoms in both neutral and oxidized states to rationalize the reactive sites and find that the grafting process takes place on the nanotube sidewall. The appearance of a new aliphatic C–C band, disappearance of peaks characteristic to vinylidene groups, and the apparition of two $-CH_2$ features in the infrared vibrational frequencies further supported the covalent bonding of OVK vinylidene groups with the SWCNT.

5.6
Summary

Practical applications of CNTs critically depend on their properties. Since it is not practically feasible to grow the nanotube with specific physical property at the present, engineering the properties of as-grown CNTs through functionalization has been an important process. Theoretical investigations, as introduced in this chapter, have indicated that it is possible to attach a wide range of functional groups such as fluorine, carboxyl, amine, amide, etc., through covalent bonds and chloroform, metalloporphyrin complexes, amino acids, etc., through noncovalent bonds on the sidewall of CNTs. Functionalization of CNTs through encapsulation of organic molecules can lead to the realization of p- and n-type doping of CNTs

that are essential for molecular electronic applications. In addition, the functionalization of CNTs via the introduction of radicals or anions serves as initiators for the subsequent grafting of polymers onto CNTs.

References

1 Geng, H., Rosen, R., Zheng, B., Shimoda, H., Fleming, L., Liu, J., and Zhou, O. (2002) *Adv. Mater.*, **14**, 1387.
2 Gong, X., Liu, J., Baskaran, S., Voise, R.D., and Young, J.S. (2000) *Chem. Mater.*, **12**, 1049.
3 Schadler, L.S., Giannaris, S.C., and Ajayan, P.M. (1998) *Appl. Phys. Lett.*, **73**, 3842.
4 Viswanathan, G., Chakrapani, N., Yang, H., Wei, B., Chung, H., Cho, K., Ryu, C.Y., and Ajayan, P.M. (2003) *J. Am. Chem. Soc.*, **125**, 9258.
5 Dieckmann, G.R., Dalton, A.B., Johnson, P.A., Razal, J., Chen, J., Giordano, G.M., Munoz, E., Musselman, I.H., Baughman, R.H., and Draper, R.K. (2003) *J. Am. Chem. Soc.*, **125**, 1770.
6 Zhu, W.H., Minami, N., Kazaoui, S., and Kim, Y. (2004) *J. Mater. Chem.*, **14**, 1924.
7 Xiao, K.Q. and Zhang, L.C. (2005) *J. Mater. Sci.*, **40**, 6513.
8 Meuer, S., Braun, L., and Zentel, R. (2009) *Macromol. Chem. Phys.*, **210**, 1528.
9 Homenick, C.M., Lawson, G., and Adronov, A. (2007) *Polym. Rev.*, **47**, 265.
10 Qin, S.H., Qin, D.Q., Ford, W.T., Resasco, D.E., and Herrera, J.E. (2004) *Macromolecules*, **37**, 752.
11 Hohenberg, P., and Kohn, W. (1964) *Phys. Rev. B*, **136**, B864.
12 Kohn, W., and Sham, L.J. (1965) *Phys. Rev.*, **140**, 1133.
13 Perdew, J.P. and Zunger, A. (1981) *Phys. Rev. B*, **23**, 5048.
14 Grimme, S., Antony, J., Schwabe, T., and Muck-Lichtenfeld, C. (2007) *Org. Biomol. Chem.*, **5**, 741.
15 Becke, A.D. (1988) *Phys. Rev. A*, **38**, 3098.
16 Becke, A.D. (1993) *J. Chem. Phys.*, **98**, 5648.
17 Lee, C.T., Yang, W.T., and Parr, R.G. (1988) *Phys. Rev. B*, **37**, 785.
18 Vosko, S.H., Wilk, L., and Nusair, M. (1980) *Can. J. Phys.*, **58**, 1200.
19 D'Souza, F., Zandler, M.E., Smith, P.M., Deviprasad, G.R., Arkady, K., Fujitsuka, M., and Ito, O. (2002) *J. Phys. Chem. A*, **106**, 649.
20 Tersoff, J. (1986) *Phys. Rev. Lett.*, **56**, 632.
21 Tersoff, J. (1989) *Phys. Rev. B*, **39**, 5566.
22 Brenner, D.W. (1990) *Phys. Rev. B*, **42**, 9458.
23 Brenner, D.W., Shenderova, O.A., Harrison, J., Stuart, S.J., Ni, B., and Sinnott, S. (2002) *J. Phys. Condens. Matter*, **14**, 783.
24 Mylvaganam, K. and Zhang, L. (2004) *Carbon*, **42**, 2025.
25 Mylvaganam, K. and Zhang, L.C. (2006) *Nanotechnology*, **17**, 410.
26 Binkley, J.S., Pople, J.A., and Hehre, W.J. (1980) *J. Am. Chem. Soc.*, **102**, 939.
27 Srivastava, D., Brenner, D.W., Schall, J.D., Ausman, K.D., Yu, M., and Ruoff, R. (1999) *J. Phys. Chem. B*, **103**, 4330.
28 Nakajima, T., Kasamatsu, S., and Matsuo, Y. (1996) *Eur. J. Solid State Inorg. Chem.*, **33**, 831.
29 Jaffe, R.L. (2003) *J. Phys. Chem. B*, **107**, 10378.
30 Bauschlicher, C.W. (2000) *Chem. Phys. Lett.*, **322**, 237.
31 Bauschlicher, C.W. (2001) *Nano Lett.*, **1**, 223.
32 Maseras, F. and Morokuma, K. (1995) *J. Comput. Chem.*, **16**, 1170.
33 Taylor, R., Holloway, J.H., Hope, E.G., Avent, A.G., Langley, G.J., Dennis, T.J., Hare, J.P., Kroto, H.W., and Walton, D.R.M. (1992) *J. Chem. Soc. Chem. Commun.*, 665.
34 Boul, P.J., Liu, J., Mickelson, E.T., Huffman, C.B., Ericson, L.M., Chiang, I.W., Smith, K.A., Colbert, D.T., Hauge, R.H., Margrave, J.L., and Smalley, R.E. (1999) *Chem. Phys. Lett.*, **310**, 367.
35 Mickelson, E.T., Chiang, I.W., Zimmerman, J.L., Boul, P.J., Lozano, J., Liu, J., Smalley, R.E., Hauge, R.H., and Margrave, J.L. (1999) *J. Phys. Chem. B*, **103**, 4318.
36 Veloso, M.V., Souza, A.G., Mendes, J., Fagan, S.B., and Mota, R. (2006) *Chem. Phys. Lett.*, **430**, 71.
37 Mercuri, F. and Sgamellotti, A. (2007) *Inorg. Chim. Acta*, **360**, 785.
38 Mercuri, F. and Sgamellotti, A. (2006) *J. Phys. Chem. B*, **110**, 15291.
39 Vaska, L. (1963) *Science*, **140**, 809.
40 Clark, M., Cramer, R.D., and Vanopdenbosch, N. (1989) *J. Comput. Chem.*, **10**, 982.
41 Perdew, J.P. (1986) *Phys. Rev. B*, **33**, 8822.
42 Banerjee, S. and Wong, S. (2002) *Nano Lett.*, **2**, 49.
43 Mylvaganam, K. and Zhang, L.C. (2004) *J. Phys. Chem. B*, **108**, 15009.
44 Girao, E.C., Liebold-Ribeiro, Y., Batista, J.A., Barros, E.B., Fagan, S.B., Mendes, J., Dresselhaus, M.S., and Souza, A.G. (2010) *Phys. Chem. Chem. Phys.*, **12**, 1518.
45 Bonnett, R. (1995) *Chem. Soc. Rev.*, **24**, 19.
46 Zhao, J.X. and Ding, Y.H. (2008) *J. Phys. Chem. C*, **112**, 11130.
47 Perdew, J.P., Burke, K., and Ernzerhof, M. (1996) *Phys. Rev. Lett.*, **77**, 3865.
48 Wang, Y.B. and Lin, Z.Y. (2003) *J. Am. Chem. Soc.*, **125**, 6072.
49 Chen, R.J., Bangsaruntip, S., Drouvalakis, K.A., Kam, N.W.S., Shim, M., Li, Y.M., Kim, W., Utz, P.J., and Dai, H.J. (2003) *Proc. Natl. Acad. Sci. USA*, **100**, 4984.
50 Zorbas, V., Smith, A.L., Xie, H., Ortiz-Acevedo, A., Dalton, A.B., Dieckmann, G.R., Draper, R.K., Baughman, R.H., and Musselman, I.H. (2005) *J. Am. Chem. Soc.*, **127**, 12323.
51 Rajesh, C., Majumder, C., Mizuseki, H., and Kawazoe, Y. (2009) *J. Chem. Phys.*, **130**, 124911.
52 Lu, J., Nagase, S., Yu, D.P., Ye, H.Q., Han, R.S., Gao, Z.X., Zhang, S., and Peng, L.M. (2004) *Phys. Rev. Lett.*, **93**, 116804.
53 Sa, N., Wang, G., Yin, B., and Huang, Y. (2008) *Physica E*, **40**, 2396.
54 Ederle, Y. and Mathis, C. (1997) *Macromolecules*, **30**, 4262.
55 Patil, A.O. and Brois, S.J. (1997) *Polymer*, **38**, 3423.
56 Kong, H., Gao, C., and Yan, D.Y. (2004) *J. Am. Chem. Soc.*, **126**, 412.
57 Shaffer, M.S.P. and Koziol, K. (2002) *Chem. Commun.*, 2074.
58 Mylvaganam, K. and Zhang, L.C. (2004) *J. Phys. Chem. B*, **108**, 5217.
59 Mulliken, R.S. (1955) *J. Chem. Phys.*, **23**, 1833.
60 Mylvaganam, K. and Zhang, L.C. (2006) *Key Eng. Mater.*, **312**, 217.
61 Napo, K., Chand, S., Bernede, J.C., Safoula, G., and Alimi, K. (1992) *J. Mater. Sci.*, **27**, 6219.
62 Safoula, G., Touihri, S., Bernede, J.C., Jamali, M., Rabiller, C., Molinie, P., and Napo, K. (1999) *Polymer*, **40**, 531.
63 Zaidi, B., Bouzayen, N., Wery, J., and Alimi, K. (2010) *J. Mol. Struct.*, **971**, 71.
64 Dewar, M.J.S., Zoebisch, E.G., Healy, E.F., and Stewart, J.J.P. (1985) *J. Am. Chem. Soc.*, **107**, 3902.
65 Wongchoosuk, C., Udomvech, A., and Kerdcharoen, T. (2009) *Curr. Appl. Phys.*, **9**, 352.